

## THE STRUCTURE OF THE DoAr 25 CIRCUMSTELLAR DISK

SEAN M. ANDREWS<sup>1</sup>, A. M. HUGHES, D. J. WILNER, AND CHUNHUA QI  
Harvard-Smithsonian Center for Astrophysics, 60 Garden Street, Cambridge, MA 02138  
*Draft version November 5, 2018*

### ABSTRACT

We present high spatial resolution ( $\lesssim 0''.3 \approx 40$  AU) Submillimeter Array observations of the  $865 \mu\text{m}$  continuum emission from the circumstellar disk around the young star DoAr 25. Despite its bright millimeter emission, this source exhibits only a comparatively small infrared excess and low accretion rate, suggesting that the material and structural properties of the inner disk may be in an advanced state of evolution. A simple model of the physical conditions in the disk is derived from the submillimeter visibilities and the complete spectral energy distribution using a Monte Carlo radiative transfer code. For the standard assumption of a homogeneous grain size distribution at all disk radii, the results indicate a shallow surface density profile,  $\Sigma \propto r^{-p}$  with  $p \approx 0.34$ , significantly less steep than a steady-state accretion disk ( $p = 1$ ) or the often adopted minimum mass solar nebula ( $p = 1.5$ ). Even though the total mass of material is large ( $M_d \approx 0.10 M_\odot$ ), the densities inferred in the inner disk for such a model may be too low to facilitate any mode of planet formation. However, alternative models with steeper density gradients ( $p \approx 1$ ) can explain the observations equally well if substantial grain growth in the planet formation region ( $r \leq 40$  AU) has occurred. We discuss these data in the context of such models with dust properties that vary with radius and highlight their implications for understanding disk evolution and the early stages of planet formation.

*Subject headings:*

### 1. INTRODUCTION

The details of the planet formation process in its early stages are largely determined by the physical conditions in the disk around the host star. The densities, temperatures, material content, and structure of this gas and dust reservoir critically influence the mechanisms and efficiencies of the assembly of a planetesimal population, as well as its subsequent growth and dynamical evolution. Spatially resolved observations of disks at millimeter wavelengths provide unique access to these physical conditions, including in particular the spatial distribution of mass (e.g., Wilner & Lay 2000). Such constraints on the physical structure of disks around young ( $\sim 1$  Myr) T Tauri stars are expected to offer a glimpse at the relatively pristine *initial* conditions available for planet formation (Beckwith & Sargent 1996).

However, recent observations of some disks raise questions about how pristine or initial these conditions really are, even at such young ages. A small collection of “transition” disks show pronounced dips in their infrared spectral energy distributions (SED) which suggest that large inner holes or gaps have been cleared (e.g., Calvet et al. 2005; Espaillat et al. 2007); a scenario confirmed in some cases by direct imaging (Piétu et al. 2006; Hughes et al. 2007; Brown et al. 2008). Although less dramatic, a separate population of disks with relatively faint infrared SED excesses (although without distinct SED gaps) but bright millimeter emission can be interpreted as evidence for substantial particle growth – and thus diminished grain emissivity – in the inner disk (Lada et al. 2006; Najita et al. 2007). These indicators suggest that some fraction of  $\sim 1$  Myr-old disks have already made significant progress along the path toward making planets.

In this Letter, we use high spatial resolution submillimeter observations to help interpret the physical conditions in the disk around DoAr 25. Located in the L1688 dark cloud in Ophiuchus ( $d \approx 145$  pc; Makarov 2007), the DoAr 25 disk has a comparatively small infrared excess and accretion rate ( $\dot{M} \sim 10^{-10}$ – $10^{-9} M_\odot \text{ yr}^{-1}$ ; Muzerolle et al. 1998; Natta et al. 2006), but bright millimeter emission (Andrews & Williams 2007b). Following a description of the observations and their calibration in §2, we utilize a standard disk model and radiative transfer calculations to estimate the disk structure and mass distribution in §3. We discuss the results in the contexts of particle growth and planet formation in §4.

### 2. OBSERVATIONS AND DATA REDUCTION

DoAr 25 ( $\alpha = 16^{\text{h}}26^{\text{m}}23^{\text{s}}.68$ ,  $\delta = -24^\circ 43' 14''.1$  [J2000]) was observed in the “very extended” configuration of the Submillimeter Array (SMA; Ho et al. 2004) on 2007 May 26 and June 17 in exceptional conditions, with zenith optical depths of  $< 0.06$  at 225 GHz. In this arrangement, the 8 SMA antennas (6 m diameter each) span physical baselines up to 508 m. The observations cycled between DoAr 25 and two quasars (J1517–243 and J1626–298) on 10 minute intervals. The raw visibilities were calibrated with the MIR package. Passband calibration was conducted with bright quasars (3C273, 3C279), and complex gain calibration was performed with J1626–298. MWC 349 and Callisto were used to set the absolute flux scale, which is accurate to  $\sim 10\%$ . Data from both nights and each of the two 2 GHz sidebands were combined. Using J1517–243 as a consistency check on the phase transfer, we estimate that phase noise and baseline errors generate an effective seeing of  $\lesssim 0''.1$ .

Additional observations in the compact and extended SMA configurations (baselines of  $\sim 15$ – $200$  m) were obtained in 2006 (see Andrews & Williams 2007a). The

<sup>1</sup> Hubble Fellow

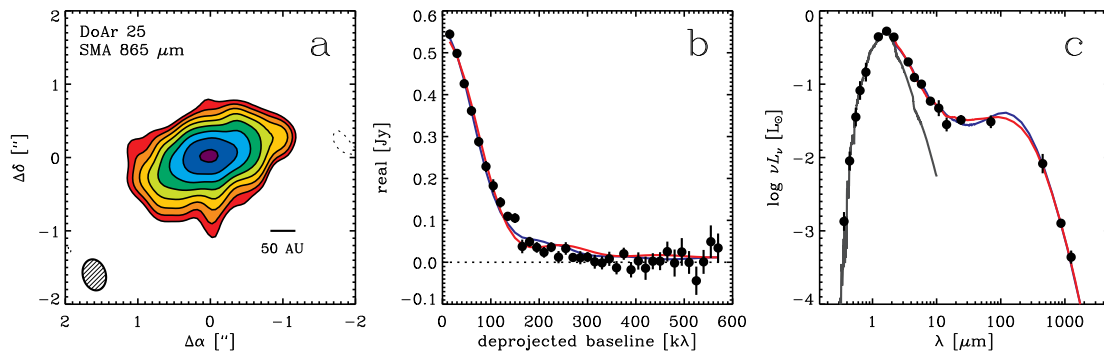


FIG. 1.— (left) High resolution SMA image of the 865  $\mu\text{m}$  continuum emission from the DoAr 25 disk. Contours start at 7.5 mJy beam $^{-1}$  ( $3\sigma$ ) and increase by factors of  $\sqrt{2}$ . The synthesized beam size is shown in the lower left corner. (middle) The elliptically-averaged 865  $\mu\text{m}$  visibilities (the real part) as a function of the deprojected baseline length. (right) The DoAr 25 SED, where the ordinate corresponds to  $4\pi d^2 \nu F_\nu$ . Optical photometry is from Vrba et al. (1993, *UBV*) and Wilking et al. (2005, *RI*). Infrared data are from 2MASS (Cutri et al. 2003), the *Spitzer Space Telescope* (L. E. Allen 2007, *private communication*), Barsony et al. (2005), and Bontemps et al. (2001). Millimeter fluxes are from Dent et al. (1998), this paper, and André & Montmerle (1994). Error bars include uncertainties in the absolute flux scales. The grey curve shows the Kurucz model adopted as the input stellar radiation source for the radiative transfer modeling. Overlaid on the visibility and SED panels are the model disk behaviors for a standard grain size distribution (red: §3) and an alternative distribution (blue) with grain growth (and reduced emissivity) in the inner disk ( $r < 40$  AU; §4).

data show excellent consistency between all configurations on overlapping spatial scales. All continuum data were combined to provide visibilities at an effective frequency of 346.9 GHz (865  $\mu\text{m}$ ). For the 2006 data, we simultaneously observed the CO  $J=3-2$  transition at 345.796 GHz with a spectral resolution of 0.70 km s $^{-1}$ . The MIRIAD package was utilized for the standard tasks of Fourier inversion, deconvolution, and imaging of the calibrated visibilities. A submillimeter continuum map was generated with a Briggs robust=0.25 weighting scheme, providing a synthesized beam FWHM of  $0''.43 \times 0''.32$  at a position angle (PA) of  $15^\circ$ .

### 3. RESULTS

Figure 1a shows a high spatial resolution 865  $\mu\text{m}$  continuum image of the DoAr 25 disk. An elliptical Gaussian fit to the visibilities indicates a well-resolved source with an integrated flux density of  $563 \pm 3$  mJy (not including the calibration uncertainty) and an inclination of  $62 \pm 3^\circ$  at a PA of  $111 \pm 3^\circ$ . The SMA visibilities are presented in Figure 1b, elliptically averaged after their deprojection based on the above geometry (see Lay et al. 1997). The visibilities drop off steeply, suggesting a shallow gradient in the radial surface brightness profile of the disk. The SED for DoAr 25 is shown in Figure 1c, using data compiled from the literature. A relatively small thermal excess is noted above the stellar photosphere out to mid-infrared wavelengths, before the SED picks up to show some of the brightest millimeter emission of all the T Tauri disks in Ophiuchus (Andrews & Williams 2007b).

For a quantitative view of the physical conditions in the DoAr 25 disk, we attempted to reproduce the full SED and SMA visibilities with the 2-D axisymmetric Monte Carlo radiative transfer code RADMC (v3.1, C. P. Dullemond 2007, *private communication*). This code utilizes the algorithm developed by Bjorkman & Wood (2001) to compute temperatures in a circumstellar medium heated solely by stellar irradiation and with a density structure

$$\rho(r, \theta) = \frac{\Sigma}{\sqrt{2\pi}H} \exp\left[-\left(\frac{r \cos \theta}{\sqrt{2}H}\right)^2\right], \quad (1)$$

where the radial coordinate ( $r$ ) runs from the dust sub-

limation radius to an outer boundary ( $R_d$ ), the angular coordinate ( $\theta$ ) runs from the rotation axis ( $\theta = 0$ ) to the midplane ( $\theta = \pi/2$ ), and the surface density and scale height vary with radius as power laws ( $\Sigma = \Sigma_0(r/R_d)^{-p}$  and  $H = H_0(r/R_d)^h$ ). Aside from some minor coordinate conventions, this disk structure model is identical to others commonly used in the literature (e.g., Chiang & Goldreich 1997). The code itself was described by Dullemond & Dominik (2004), but now includes a diffusion algorithm that is employed for grid locations with poor photon statistics (i.e., near the disk midplane).

The central illumination source was a Kurucz model (gray curve in Fig. 1c) fixed to match the properties of the star and optical SED: a K5 spectral type ( $T_{\text{eff}}=4250$  K),  $L_*=1.3L_\odot$ , and  $A_V=2.9$  (Wilking et al. 2005). We initially adopted the emissivity properties provided by D’Alessio et al. (2001), for a dust grain size ( $a$ ) distribution that varies as  $n(a) \propto a^{-3.5}$  between  $a_{\text{min}}=0.005$   $\mu\text{m}$  and  $a_{\text{max}}=1$  mm. These emissivities are essentially identical to the standard disk values used at millimeter wavelengths (Beckwith et al. 1990). With this information, we ran the radiative transfer code over a grid of 5 free parameters that characterize the disk structure:  $R_d$ ,  $p$ ,  $h$ , and the normalizations of  $\Sigma$  (i.e., the disk mass,  $M_d$ ) and  $H$ . For each point in the grid a model SED and 865  $\mu\text{m}$  visibilities were generated with a ray-tracing program, assuming the above orientation.

The best-fit model parameter values estimated from minimizing  $\chi^2$  are  $R_d = 310$  AU,  $p = 0.34$ ,  $h = 1.11$ ,  $M_d = 0.10 M_\odot$ , and  $H = 28$  AU (at  $R_d$ ). The synthetic SED and visibilities for a model with these parameters are shown in red in Figure 1. The reduced  $\chi^2$  value comparing the best-fit model and the data shown in Fig. 1b and 1c was  $\sim 2$ , primarily due to difficulty reproducing the mid-infrared spectrum in detail. The formal  $1\sigma$  parameter uncertainties are  $\sim 15$  AU for  $R_d$ ,  $\sim 0.01 M_\odot$  for  $M_d$ , and  $\sim 5$  AU for  $H$  (at  $R_d$ ), while  $p$  can range from 0.2–0.4 and the flared shape of the disk can run as low as  $h \approx 1.07$  (but not higher than the best-fit value without over-producing infrared emission).

As an *a posteriori* test of the derived disk properties, Figure 2 compares an optical (0.6  $\mu\text{m}$ ) *Hubble Space Telescope* (*HST*; WFPC2/F606W) image of starlight scat-

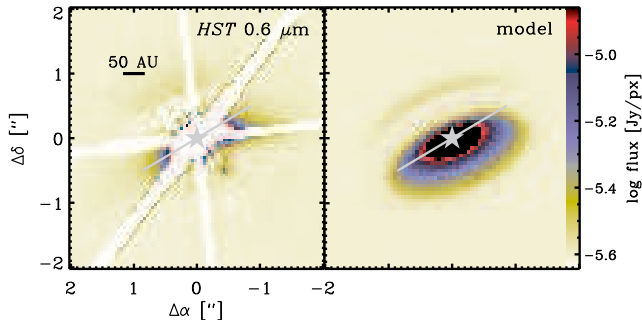


FIG. 2.— (left) An optical *HST* image (F606W,  $\sim 0.6 \mu\text{m}$ ) of starlight scattered off the surface of the DoAr 25 disk. (right) The scattered light image predicted from the best-fit model parameters described in §3, based solely on the SMA visibilities and the SED. The stellar position is labeled with a star symbol, a gray line marks the orientation of the disk major axis, and a logarithmic brightness scale is shown on the right. While the model does not include direction-dependent scattering (and is therefore not used in the structure determination), the comparison with the *HST* data confirms the size scales, orientation, and general disk geometry that were derived from the SMA data alone.

tered off the DoAr 25 disk surface (Stapelfeldt et al. 2008) with a RADMC model prediction corresponding to the above parameters. Because this version of RADMC only treats isotropic scattering, a quantitative comparison with the data is unjustified. However, it is clear that the best-fit model is in good qualitative agreement with the disk orientation and geometry as traced by both the scattered flux scale and the location and intensity of the dust lane marking the midplane.

While not shown here, channel maps of the CO  $J=3-2$  transition from the SMA data (with a  $1''.8 \times 1''.6$  beam at PA =  $4^\circ$ ) exhibit two distinct patches of weak line emission separated by  $\sim 4 \text{ km s}^{-1}$  toward DoAr 25, centered on the local cloud velocity ( $V_{\text{LSR}} = 3.3 \text{ km s}^{-1}$ ). Single-dish mapping of the Ophiuchus clouds in the CO  $J=1-0$  transition shows a bright, optically thick line with a FWHM of  $\sim 3 \text{ km s}^{-1}$  coincident with the DoAr 25 position (Ridge et al. 2006). Unfortunately, this suggests that the line emission from the disk remains substantially contaminated by confusion with the more extended molecular cloud.

#### 4. DISCUSSION

The spatial distribution of mass, characterized by the surface density index  $p$ , is a critical diagnostic for understanding the material evolution and planet formation potential of a disk. It reflects the disk viscosity and therefore provides an observable indication of the evolution timescale dictated by the accretion process and angular momentum conservation. Moreover, the mass distribution will influence the composition and architecture of a developing planetary system. By comparing the decay of accretion rates over time with models that use a simple prescription for the turbulent viscosity, Hartmann et al. (1998) argue for a typical value  $p=1$ . A steeper gradient ( $p=1.5$ ) is invoked to account for the mass distribution in the solar system, once augmented to cosmic abundances and smeared into annuli (the minimum mass solar nebula, or MMSN; Weidenschilling 1977).

The low value of  $p$  derived for the DoAr 25 disk would have important implications for understanding its evolution. In the Hartmann et al. (1998) prescription for a viscous accretion disk, such a low value of  $p$  would produce a

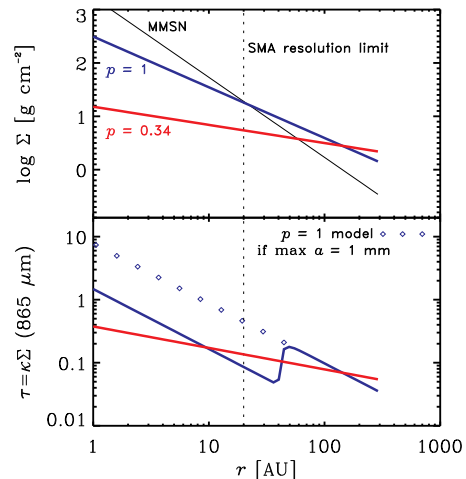


FIG. 3.— (top) The radial surface density profile ( $\Sigma$ ; gas+dust) for the best-fit model described in §3 (red) and the toy model with large grains in the inner disk described in §4 (blue). The latter is decomposed into two grain populations, with  $a_{\text{max}} = 1 \text{ mm}$  outside 40 AU and 1 m (both from D’Alessio et al. 2001) inside that radius. The minimum mass solar nebula (MMSN) density profile is shown in black for comparison. (bottom) The radial profile of the 865  $\mu\text{m}$  continuum optical depth ( $\tau = \kappa\Sigma$ ; where  $\kappa$  represents the material emissivity) for the same models. The open diamonds track the optical depth that would be expected if the standard ( $a_{\text{max}} = 1 \text{ mm}$ ) grain size distribution emissivity were adopted everywhere in the disk for the steep density gradient ( $p = 1$ ) model. The SMA resolution limit for these data is marked with a vertical dotted line.

significantly diminished mass accretion rate onto the star over most of the disk lifetime, perhaps lower by a factor of  $\sim 2$  compared to the canonical disk with  $p = 1$ . This is in reasonable agreement with constraints on  $\dot{M}$ , which vary from low ( $5 \times 10^{-9} M_{\odot} \text{ yr}^{-1}$ ; Muzerolle et al. 1998) to negligible values ( $< 5 \times 10^{-10} M_{\odot} \text{ yr}^{-1}$ ; Natta et al. 2006). In essence, the accretion process is less efficient in a disk with a shallow density gradient. The same could be said about the formation of planets in such a disk. In spite of the large  $M_d$ , the inner disk densities implied by this low- $p$  model are more than an order of magnitude smaller than those required by planet formation models (e.g., Hubickyj et al. 2005, also note that even though  $M_d/M_* \approx 0.18$ , the Toomre stability criterion holds at all radii in this model). Previous millimeter observations of disks have generally found large  $p$  ( $\geq 0.7$ ; e.g., Wilner et al. 1996; Andrews & Williams 2007a; Piétu et al. 2006; Hamidouche et al. 2006), although the derived value for DoAr 25 lies in the low end of a wide distribution; the variety of modeling techniques and spatial resolutions in those studies make direct comparisons difficult.

Of course, there are alternative interpretations of the observed DoAr 25 disk properties that do not call for such a small density gradient. The absence of a pronounced dip feature in the infrared SED or an apparent “hole” in the submillimeter surface brightness distribution can effectively rule out a substantially cleared inner region like those those in transition disks. However, because the millimeter continuum emission traces the optical depth in the disk – the *product* of the density structure and the dust emissivity – the observed shallow brightness profile could be explained equally well with steep density gradients ( $p \geq 1$ ) if the emissivity compensates by decreasing

toward small radii. For the models described in §3 (and generally in the literature), the grain size distribution is assumed to be spatially uniform throughout the disk. In reality, particle sizes in the inner disk might be larger than in the outer disk because the collisional growth timescale is shorter for higher densities and orbital velocities (e.g., Dullemond & Dominik 2005; Garaud 2007, and references therein). D’Alessio et al. (2001) show that the millimeter emissivity quickly decreases as  $a_{\max}$  grows beyond  $\sim 1$  mm. Therefore, a shorter grain growth timescale in the inner disk would naturally produce an emissivity that decreases at smaller radii.

To illustrate the effects this would have observationally, we constructed a crude toy model that has the standard steady-state accretion disk density profile ( $p = 1$ ), but allows particles with a factor of  $\sim 5$  smaller emissivity (at  $865 \mu\text{m}$ ; corresponding to  $a_{\max} \approx 1$  m) to account for essentially all of the mass on solar system scales ( $r \leq 40$  AU). As shown in blue in Figure 1, models that mimic grain growth can reproduce both the DoAr 25 SED behavior and the shallow millimeter brightness profile fairly well. However, given the additional freedom that comes with more model parameters, the data do not uniquely distinguish values of inputs like  $a_{\max}$ . Different values can be accommodated by adjusting the relative abundances and locations of the grain populations. Figure 3 shows the radial distributions of  $\Sigma$  and the  $865 \mu\text{m}$  optical depth for both this toy model and the more standard prescription adopted in §3. While the details in such an *ad hoc* demonstration model are unimportant, the lower panel of Figure 3 highlights the salient point: a decrease in the inner disk emissivity can effectively mask a steep density gradient.

There is considerable evidence from the shape of millimeter continuum spectra that disk emissivities have been modified by substantial particle growth, albeit in an average sense due to limited spatial resolution (e.g., Beckwith & Sargent 1991; Testi et al. 2001, 2003; Wilner et al. 2005; Rodmann et al. 2006). DoAr 25 has a

fairly typical long-wavelength SED shape ( $n = 2.7 \pm 0.2$ , where  $F_\nu \propto \nu^n$ ) for a T Tauri star. High spatial resolution observations at multiple frequencies (from  $\sim 40$ –400 GHz) can potentially disentangle the millimeter SED shape ( $n$ ; i.e., colors) in the evolved inner disk from the more primordial material at larger radii. Such data could be used to empirically reconstruct the shape of the emissivity spectrum as a function of location in the disk, which could subsequently be modeled to map out the constituent grain populations.

If the properties of disks like DoAr 25 are caused by particle growth in the inner disk, they can be considered less-evolved versions of “transition” disks, with larger remnant optical depths in their inner holes (effectively muting out the signature dip in the SED noted for transition disks). It would be interesting to model high-resolution millimeter observations of similar disks and see if shallow density gradients (low  $p$ ) are commonly inferred when assuming a standard grain size distribution. If that is the case, such results could be a signature that a few percent of  $\sim 1$  Myr-old disks are already well on their way to making planets.

We are grateful to Lori Allen, Karl Stapelfeldt, John Krist, Melissa McClure, and Dan Watson for kindly sharing their data prior to publication, Paola D’Alessio for providing dust emissivity tables, and especially to Kees Dullemond and Roy van Boekel for all of their prompt and patient assistance with the RADMC code. The SMA is a joint project between the Smithsonian Astrophysical Observatory and the Academia Sinica Institute of Astronomy and Astrophysics and is funded by the Smithsonian Institution and the Academia Sinica. Support for this work was provided by NASA through Hubble Fellowship grant #HF-01203.01-A awarded by the Space Telescope Science Institute, which is operated by the Association of Universities for Research in Astronomy, Inc., for NASA, under contract NAS 5-26555.

#### REFERENCES

- André, P., & Montmerle, T. 1994, *ApJ*, 420, 837  
 Andrews, S. M., & Williams, J. P. 2007, *ApJ*, 659, 705 (2007a)  
 ——— 2007, *ApJ*, 671, 1800 (2007b)  
 Barsony, M., Ressler, M. E., & Marsh, K. A. 2005, *ApJ*, 630, 381  
 Beckwith, S. V. W., Sargent, A. I., Chini, R., & Güsten, R. 1990, *AJ*, 99, 924  
 Beckwith, S. V. W., & Sargent, A. I. 1991, *ApJ*, 381, 250  
 ——— 1996, *Nature*, 383, 139  
 Bjorkman, J. E., & Wood, K. 2001, *ApJ*, 554, 615  
 Bontemps, S., et al. 2001, *A&A*, 372, 173  
 Brown, J. M., Blake, G. A., Qi, C., Dullemond, C. P., & Wilner, D. J. 2008, *ApJ*, in press  
 Calvet, N., et al. 2005, *ApJ*, 630, L185  
 Chiang, E. I., & Goldreich, P. 1997, *ApJ*, 490, 368  
 Cutri, R. M., et al. 2003, 2MASS All-Sky Point Source Catalog (Pasadena: IPAC)  
 D’Alessio, P., Calvet, N., & Hartmann, L. 2001, *ApJ*, 553, 321  
 Dent, W. R. F., Matthews, H. E., & Ward-Thompson, D. 1998, *MNRAS*, 301, 1049  
 Dullemond, C. P., & Dominik, C. 2004, *A&A*, 417, 159  
 ——— 2005, *A&A*, 434, 971  
 Espaillat, C., et al. 2007, *ApJ*, 670, L135  
 Garaud, P. 2007, *ApJ*, 671, 2091  
 Hamidouche, M., Looney, L. W., & Mundy, L. G. 2006, *ApJ*, 651, 321  
 Hartmann, L., Calvet, N., Gullbring, E., & D’Alessio, P. 1998, *ApJ*, 495, 385  
 Ho, P. T. P., Moran, J. M., & Lo, K. Y. 2004, *ApJ*, 616, L1  
 Hubickyj, O., Bodenheimer, P., & Lissauer, J. J. 2005, *Icarus*, 179, 415  
 Hughes, A. M., Wilner, D. J., Calvet, N., D’Alessio, P., Claussen, M. J., & Hogerheijde, M. R. 2007, *ApJ*, 664, 536  
 Lada, C. J., et al. 2006, *AJ*, 131, 1574  
 Lay, O. P., Carlstrom, J. E., & Hills, R. E. 1997, *ApJ*, 489, 917  
 Makarov, V. V. 2007, *ApJ*, 670, 1225  
 Muzerolle, J., Hartmann, L., & Calvet, N. 1998, *AJ*, 116, 2965  
 Najita, J. R., Strom, S. E., & Muzerolle, J. 2007, *MNRAS*, 378, 369  
 Natta, A., Testi, L., & Randich, S. 2006, *A&A*, 452, 245  
 Piétu, V., Dutrey, A., Guilloteau, S., Chappillon, E., & Pety, J. 2006, *A&A*, 460, L43  
 Ridge, N. A., et al. 2006, *AJ*, 131, 2921  
 Rodmann, J., Henning, T., Chandler, C. J., Mundy, L. G., & Wilner, D. J. 2006, *A&A*, 446, 211  
 Stapelfeldt, K., et al. 2008, in preparation  
 Testi, L., Natta, A., Shepherd, D. S., & Wilner, D. J. 2001, *ApJ*, 554, 1087  
 ——— 2003, *A&A*, 403, 323  
 Vrba, F. J., Coyne, G. V., & Tapia, S. 1993, *AJ*, 105, 1010  
 Weidenschilling, S. J. 1977, *Ap&SS*, 51, 153  
 Wilking, B. A., Meyer, M. R., Robinson, J. G., & Greene, T. P. 2005, *AJ*, 130, 1733  
 Wilner, D. J., Ho, P. T. P., & Rodriguez, L. F. 1996, *ApJ*, 470, L117

- Wilner, D. J., & Lay, O. P. 2000, in *Protostars & Planets IV*, eds. V. Mannings, A. P. Boss, & S. S. Russell (Tucson: Univ. Arizona Press), 509
- Wilner, D. J., D'Alessio, P., Calvet, N., Claussen, M. J., & Hartmann, L. 2005, *ApJ*, 626, L109